Biochemistry

pubs.acs.org/biochemistry Article

The Human Cytochrome *c* Domain-Swapped Dimer Facilitates Tight Regulation of Intrinsic Apoptosis

Harmen B. B. Steele, Margaret M. Elmer-Dixon, James T. Rogan, J. B. Alexander Ross, and Bruce E. Bowler*

Cite This: https://dx.doi.org/10.1021/acs.biochem.0c00326 Read Online

ABSTRACT: Oxidation of cardiolipin (CL) by cytochrome *c* (cyt*c*) has been proposed to initiate the intrinsic pathway of apoptosis. Domain-swapped dimer (DSD) conformations of cyt*c* have been reported both by our laboratory and by others. The DSD is an alternate conformer of cyt*c* that could oxygenate CL early in apoptosis. We demonstrate here that the cyt*c* DSD has a set of properties that would provide tighter regulation of the intrinsic pathway. We show that the human DSD is kinetically more stable than horse and yeast DSDs. Circular dichroism data indicate that the DSD has a less asymmetric heme environment, similar to that seen when the monomeric protein binds to CL vesicles at high lipid:protein ratios. The dimer undergoes the alkaline conformational transition near pH 7.0, 2.5 pH units lower than that of the monomer. Data from fluorescence correlation spectroscopy and fluorescence anisotropy suggest that the alkaline transition of the DSD may act as a switch from a high affinity for CL nanodiscs at pH 7.4 to a much lower affinity at pH 8.0. Additionally, the peroxidase activity of the human DSD increases 7-fold compared to that of the monomer at pH 7 and 8, but by 14-fold at pH 6 when mixed Met80/H_2O ligation replaces the lysine ligation of the alkaline state. We also present data that indicate that cyt*c* binding shows a cooperative effect as the concentration of cyt*c* is increased. The DSD appears to have evolved into a pH-inducible switch that provides a means to control activation of apoptosis near pH 7.0.

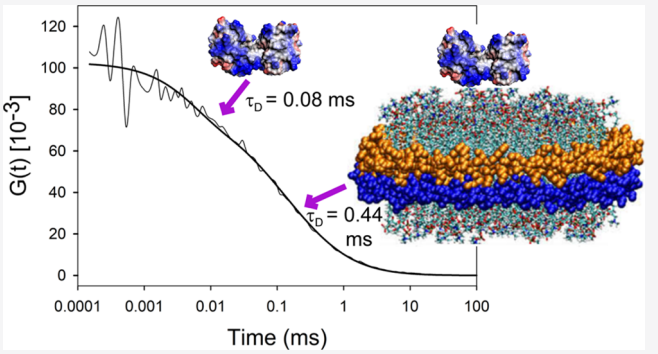

Cytochrome *c* (cyt*c*) is a soluble heme protein known for its role in the electron transport chain, shuttling electrons between $CoQH_2$-cytochrome *c* reductase (Complex 3) and cytochrome *c* oxidase (Complex 4).[1−4] However, cyt*c* has been classified as an extreme multifunctional or "moonlighting" protein because it is involved in other cellular processes besides electron transport.[5] Prominent among these moonlighting functions is its role as an initiator of the intrinsic apoptotic pathway.[6−9] In this role, cyt*c* migrates from the intermembrane space (IMS) of the mitochondria to the cytosol interacting with apoptotic protease activating factor 1 to form the apoptosome and initiate apoptosis.[10] When cyt*c*, which has a +8 net charge at neutral pH, binds the anionic phospholipid cardiolipin (CL), it gains peroxidase activity and oxidizes CL.[11−13] The oxidation of CL by cyt*c* has been implicated in permeabilizing the outer mitochondrial membrane (OMM) and in facilitating the release of cyt*c* into the cytosol because of its weaker binding to oxidized CL.[11,14,15]

CL, a potent activator of cyt*c*'s peroxidase activity,[16] comprises ∼25% of the lipids of the inner mitochondrial membrane.[17] Under normal conditions, CL is not present in the OMM.[18] Cyt*c*'s function in the electron transport chain is not affected by cyt*c*−CL interaction because the availability of CL in the IMS is lower and the local ionic strength is relatively high (150 mM), which inhibits binding.[16,19] Preceding apoptosis, CL migrates to the OMM.[12,20−23] Proapoptotic factors, including cyt*c*, are then released from the mitochondria as CL redistribution triggers lipid peroxidation and permeabilization of the OMM.[24,25]

An increasing number of domain-swapped protein dimer structures continue to be identified and are believed to have biological roles.[26] It has been shown that yeast[27] and equine[28] cyt*c* can form a domain-swapped dimer (DSD). In the yeast and horse structures, the hinge region between the two subunits is derived from highly conserved Ω-loop D (residues 70−85).[29] This loop acts as the gatekeeper to the heme, providing Met80 to the sixth coordination site of the heme.[30] The dynamics of this loop also are critical for providing access to conformers that are competent for peroxidase activity.[5] In these crystal structures, the heme is solvent-exposed and

Received: April 21, 2020
Revised: May 17, 2020
Published: May 19, 2020

https://dx.doi.org/10.1021/acs.biochem.0c00326
Biochemistry XXXX, XXX, XXX−XXX

available for peroxidase activity because the repositioned Ω-loop D leads to a loss of Met80 coordination. We have published DSD structures with lipid surrogates inhabiting a hydrophobic tube connecting the aqueous environment to the heme.[27] The binding site is located near Asn52, which was proposed to hydrogen bond to protonated CL[31] as part of the C site for CL binding to cytc. Although recent studies show that CL does not have a protonation equilibrium in the pH range corresponding to the C site,[32,33] these DSD X-ray structures with lipid bound in a well-defined cavity support the extended lipid anchorage model for cytc−CL binding that was an essential component of the C site.[31] Through docking studies based on the detergent-bound DSD structures, we have shown that linoleic acid, the predominate fatty acyl chain found in CL,[34] readily fits into this binding site for peroxidase activity.[27]

There is a growing body of evidence that DSDs of cytc can form *in vivo* and thus could be physiologically relevant. The Hirota lab has shown that *Hydrogenobacter thermophilus* cytochrome c_{552} can form DSDs and higher-order oligomers *in vivo* when expressed in *Escherichia coli*.[35] The cytoplasmic membrane of *E. coli* is composed of 20% lipids with negatively charged headgroups (CL and phosphatidylglycerol).[36] In a more recent study, the Hirota lab showed that positively charged cytochromes *c* formed DSDs when expressed in *E. coli*, whereas negatively charged cytochromes *c* did not, strongly suggesting that electrostatic interaction with the cellular membrane can catalyze (and is required for) formation of DSDs *in vivo*.[37] Studies of the formation of DSDs during folding of negatively and positively charged cytochromes *c*, in the presence of negatively charged liposomes, provided additional support for this conclusion.[37] *In vitro* formation of DSDs normally requires treatment with ethanol or detergent.[28,38−40] However, crystallized DSD variants have formed directly from monomeric cytc during crystallization,[27] and it has been shown that dimeric cytc will form spontaneously, albeit slowly, from a monomeric starting material in solution.[27] DSDs of cytc can also form during folding *in vitro*.[41] Thus, it is possible that they could also form during folding *in vivo*.

Ω-Loop D is one of the least stable substructures of cytc[42] and thus is a likely mediator of conformational rearrangements of the protein. Interestingly, rearrangement of Ω-loop D of each subunit of the DSD causes the C-terminal helix to splay out from the rest of the polypeptide chain (Figure S1),[27,28] similar to the structure proposed for the extended conformer of cytc at high lipid:protein ratios by the Pletneva lab.[43] Thus, the extended conformer observed by the Pletneva lab could facilitate formation of the DSD on CL-containing membrane surfaces. This conformational rearrangement also opens the heme site, allowing for increased peroxidase activity.[43] The equine cytc DSD has been shown to have a 5-fold increased peroxidase activity when compared with that of the monomer.[44] The rearrangement of Ω-loop D results in a larger heme cavity and faster formation of Compound I.[44] Compound I, the oxoferryl porphyrin π-cation radical, is the initial intermediate of the peroxidase reaction,[45,46] and its formation is the rate-determining step in the peroxidase reaction of the DSD of cytc.[44]

Herein, we present human cytc DSD data that support a possible functional role as a switch that evolved for controlling the initiation of the intrinsic pathway of apoptosis. Dimer dissociation data show that the human DSD is more kinetically stable than the yeast and horse DSDs. Data for the alkaline conformational transition show that the midpoint pH, $pH_{1/2}$, is near 7, dramatically lower than that of the monomer. Near $pH_{1/2}$, the DSD's binding affinity for CL nanodiscs (NDs), as measured by fluorescence correlation spectroscopy (FCS) and fluorescence anisotropy using a zinc-substituted cytc variant (Zncytc), also increases strongly. Comparing fluorescence binding data and CD binding data, we show that there appears to be a cooperative effect to the binding when the concentration of cytc is increased. Lastly, we show that the dimer has increased peroxidase activity compared to that of the monomer and that the relative increase is larger in the presence of CL NDs and at pH values below $pH_{1/2}$.

MATERIALS AND METHODS

Expression of Human Cytochrome *c*. Wild-type human cytc was expressed from the pBTR(HumanCc)[47] plasmid after transformation in Ultra BL21 (DE3) *E. coli* competent cells (EdgeBio, Gaithersburg, MD) using the manufacturer's protocol. Transformed cells were grown in Terrific Broth medium with the addition of 100 μL of Antifoam C Emulsion (Sigma A8011) per liter of culture.

Cytc extraction and purification were performed as previously described.[27,48−52] However, sonication was used in place of a French press to lyse the cells. Briefly, sonicated cell lysates were treated with 50% ammonium sulfate to precipitate contaminating proteins. CM-sepharose cation-exchange chromatography was used to further purify the protein. Samples were stored at −80 °C until they were used. Prior to experimentation, samples were thawed for cation-exchange purification with an ÄKTAprime plus instrument (GE Healthcare Life Sciences) and a HiTrap SP HP cation-exchange column (GE Healthcare 17115101). Protein samples were concentrated by ultrafiltration and oxidized with potassium ferricyanide $\{K_3[Fe(CN)_6]\}$, followed by separation of oxidized cytc from the oxidizing agent using a Sephadex G25 column.

The human cytc dimer was generated in a manner similar to previously described methods.[27,44] Briefly, after oxidation, cytc was precipitated by the addition of 80% (v/v) ethanol. Samples were then incubated at room temperature for 15 min, centrifuged for 15 min at 4 °C, flash-frozen, and lyophilized overnight. Lyophilized samples were stored at −80 °C until they were used. Samples were then resuspended in 50 mM potassium phosphate buffer (pH 7.0) to a concentration of 10 mg/mL and incubated at 37 °C for 1.5 h while being shaken. The dimer species was separated from the monomer and higher-order oligomers using a Bio-Rad Enrich SEC70 High-Resolution Size-Exclusion column (BioRad 780-1070).

Zinc-Substituted Cytochrome *c*. The zinc substitution of cytc was adapted from a previously described procedure.[53] It should be noted that this is a hazardous procedure performed in a vented fume hood with the operator wearing a respirator, an acid apron, and doubled nitrile gloves to minimize the possibility of skin exposure. Calcium gluconate gel should be available in case of skin exposure. Briefly, lyophilized cytc was mixed with HF-pyridine (70% HF) in a Teflon beaker (3 mg of cytc/mL of HF-pyridine). All samples were protected from light exposure because of the photosensitivity of the unmetalated cytc and Zncytc. The solution was stirred for 10 min, and then the reaction was quenched with 5 mL of 50 mM ammonium acetate (pH 5.0) per 10 mL of HF-pyridine. The solution was kept under a stream of nitrogen gas for 2 h followed by a 4 h dialysis against 10 mM sodium acetate (pH

https://dx.doi.org/10.1021/acs.biochem.0c00326
Biochemistry XXXX, XXX, XXX−XXX

5.0) at room temperature. Metal-free porphyrin cyt*c* was then separated from the remaining ferric cyt*c* using a CM Sepharose fast-flow ion-exchange column (GE Healthcare). Demetalated porphyrin cyt*c* was then incubated with a 100-fold excess of zinc acetate for 10 min at 70 °C while being shaken. Zinc incorporation was monitored spectroscopically: the Soret band at 423 nm sharpens dramatically, and the Q-bands at 549 and 584 nm appear (Figure S2).[54] Excess zinc acetate was removed using a G-25 Sephadex size-exclusion column.

Preparation of Cardiolipin Nanodiscs. A nanodisc (ND) is a discoidal lipid−protein complex whose shape and stability are controlled by the amphipathic α-helical membrane scaffold protein (MSP), which separates the hydrophobic tails of the bilayer from bulk water by forming a belt around the perimeter of the lipid bilayer.[55−58] The lipid:belt molar ratio is critical to ND formation: an 80:1 ratio was used for 1,2-dimyristoyl-*sn*-glycero-3-phosphocholine (DMPC), and a 25:1 ratio was used for CL. Monounsaturated tetraoleoyl-cardiolipin (TOCL) [1′,3′-bis(1,2-dioleoyl-*sn*-glycero-3-phospho)-glycerol] (Avanti 710335C) and DMPC (Avanti 850345C) were purchased from Avanti Polar Lipids (Alabaster, AL) and dissolved in high-performance liquid chromatography grade chloroform. In this study, we use tetraoleoyl-cardiolipin (TOCL) because CLs with longer unsaturated fatty acyl chains have been shown to be more efficient at binding cyt*c* and inducing peroxidase activity than CLs with shorter saturated fatty acyl chains.[59] Similar to ND preparations previously studied,[60] appropriate amounts of lipid were dried for 1−2 h under a steady stream of nitrogen gas. Lipids were then rehydrated in MSP buffer [50 mM Tris (pH 7.4), 150 mM NaCl, and 0.1% NaN_3] with 48 mM sodium cholate. The NaCl concentration was increased to 300 mM to facilitate CL ND formation. Following a 15 min cycle of sonication and vortexing, rehydrated lipids were incubated with MSP1D1 belt protein (Sigma M6574) for 30 min. Samples were then incubated with SM-2 Bio-Beads Resin (Bio-Rad 1523920) overnight at 4 °C followed by incubation for 1 h at room temperature with fresh SM-2 Bio-Beads Resin. Samples were then spun at 15K rpm for 15 min to pellet the remaining liposomes (Beckman Coulter Microfuge 18 Centrifuge). CL NDs were then purified at 4 °C using a GE Superdex 200 10/300 GL (GE17-5175-01) size-exclusion column and an ÄKTA-FPLC instrument (GE Healthcare). The running buffer was that used for titrations. Purified CL NDs were stored at 4 °C until they were used. The final concentration of CL NDs was determined using the ε_{280} of the belt protein (21430 with a His tag and 18450 without a tag[55]) and dividing by 2 because each ND is composed of two belt proteins.

Dimer Dissociation Kinetics. Human cyt*c* DSD dissociation kinetics were studied using previously published methods.[27] Briefly, following isolation of the pure dimer using the Bio-Rad Enrich SEC70 column at 4 °C in 50 mM potassium phosphate (pH 7), solutions of the dimer were incubated at 40, 45, 50, 55, and 60 °C in a Julabo F12-ED refrigerated/heating circulator. Dissociation from dimer to monomer was measured at each time point by size-exclusion chromatography of 100−150 μL aliquots using the SEC70 column. The fractions of the dimer (f_{Dimer}) and monomer (f_{Monomer}) were evaluated from their relative peak heights at 280 nm in the FPLC chromatogram. Plots of f_{Dimer} and f_{Monomer} versus time were fit to a single exponential to determine the rate constant for conversion of the dimer to the monomer (k_{DM}). Eyring plots of k_{DM} were then fit to eq 1 using a reference temperature (T_0) of 310.15 K.

$$\ln(k_{\mathrm{DM}}) = \ln\left(\frac{k_{\mathrm{B}}T}{h}\right) - \frac{\Delta H^{\ddagger}_{T_0} + \Delta C^{\ddagger}_{p}(T - T_0)}{RT} + \frac{\left[\Delta S^{\ddagger}_{T_0} + \Delta C^{\ddagger}_{p} \times \ln\left(\frac{T}{T_0}\right)\right]}{R} \quad (1)$$

where k_{B} and h are the Boltzmann and Planck constants, respectively, $\Delta H^{\ddagger}_{T_0}$ and $\Delta S^{\ddagger}_{T_0}$ are the difference in enthalpy and entropy, respectively, between the ground state and the transition state, and $\Delta C^{\ddagger}_{p}$ is the difference in heat capacity between the ground state and the transition state (TS) at constant pressure.

Alkaline Conformational Transition. The alkaline conformational transition can be followed by monitoring the weak absorbance at 695 nm (A_{695}), which reports on the Met80-heme ligation of the native state of oxidized cyt*c*.[2] Absorbance data, collected with a Beckman DU800 spectrophotometer, were corrected for baseline drift using the absorbance at 750 nm (A_{750}) yielding $A_{695\mathrm{corr}} = A_{695} - A_{750}$. The pH of samples containing 100 μM heme and 100 mM NaCl was adjusted using NaOH and HCl, using a procedure that keeps the protein concentration and NaCl concentration constant during the titration.[61] Titration measurements were performed at room temperature (22 ± 3 °C).

The midpoint pH, $\mathrm{pH}_{1/2}$, was determined by fitting plots of $A_{695\mathrm{corr}}$ versus pH to a modified form of the Henderson−Hasselbalch equation (eq 2).

$$A_{695\mathrm{corr}} = \frac{A_{\mathrm{N}} + A_{\mathrm{Alk}} \times 10^{n(\mathrm{pH}_{1/2} - \mathrm{pH})}}{1 + 10^{n(\mathrm{pH}_{1/2} - \mathrm{pH})}} \quad (2)$$

where n represents the number of protons linked to the alkaline transition, A_{N} represents $A_{695\mathrm{corr}}$ in the native state with Met80 bound to the heme, and A_{Alk} represents $A_{695\mathrm{corr}}$ in the alkaline state with a lysine from Ω-loop D bound to the heme.

Peroxidase Activity Measurements. The peroxidase activity of cyt*c* was measured at 25 ± 0.1 °C using the previously described guaiacol colorimetric assay.[30,44] Briefly, the formation of tetraguaiacol from guaiacol and hydrogen peroxide in the presence of cyt*c* was monitored at 470 nm, A_{470}, using an Applied Photophysics SX20 stopped-flow spectrometer. Working stocks of H_2O_2 (ε_{240} = 41.5 M^{-1} cm^{-1}),[62,63] guaiacol (ε_{274} = 2150 M^{-1} cm^{-1}),[64] and cyt*c* were mixed in the stopped-flow apparatus. The final solution concentrations after mixing were 1 μM heme (i.e., 1 μM monomeric cyt*c* or 0.5 μM DSD), 50 mM H_2O_2, and appropriate amounts of guaiacol in 50 mM buffer. The final CL ND concentration, where appropriate, was 1 μM. Three independent experiments were performed at each pH. Five kinetic traces were collected at each guaiacol concentration during each experiment. MatLab was used to calculate the initial velocity (greatest slope) of the A_{470} versus time data for each guaiacol concentration. The initial rate of guaiacol consumption (v) was determined by dividing the slope (dA_{470}/dt) by the extinction coefficient of tetraguaiacol (ε_{470} = 26.6 mM^{-1} cm^{-1})[65] and multiplying by 4 (four guaiacols consumed per tetraguaiacol produced). This initial rate of guaiacol consumption, v, was then divided by the concentration of cyt*c* and fit to eq 3 to obtain K_{m} and k_{cat} values:

https://dx.doi.org/10.1021/acs.biochem.0c00326
Biochemistry XXXX, XXX, XXX−XXX

$$\frac{v}{[\text{cyt}c]} = \frac{k_{\text{cat}}[\text{guaiacol}]}{K_{\text{m}} + [\text{guaiacol}]} \quad (3)$$

Circular Dichroism Spectroscopy. Stock cyt*c* samples were prepared at twice the experimental concentration and mixed in a 1:1 ratio with a CL ND solution at twice the desired final CL ND concentration to produce each data point of the titration. The experimental concentration of cyt*c* was 10 μM based on the heme absorbance (i.e., 10 μM monomer or 5 μM DSD). Samples were gently mixed by pipetting up and down and then incubated for 30 min prior to measurement. Experiments were performed in triplicate.

Soret circular dichroism (CD) spectra (350−450 nm) were acquired using an Applied Photophysics Chirascan CD spectrophotometer. Spectra were acquired using a 3 s/nm acquisition time, a 1.8 nm bandwidth, and 1 nm steps at 25 °C. Each sample was measured five times, and then the values were averaged. Spectra were smoothed using a sixth-order Savitsky−Golay filter smoothing technique.

Fluorescence Experiments with Human Cytochrome *c*. Fluorescence correlation spectroscopy (FCS) and fluorescence anisotropy measurements were obtained by time-correlated single-photon counting (TCSPC) using a PicoQuant (Berlin, Germany) MicroTime 200 time-resolved confocal fluorescence microscope in the BioSpectroscopy Core Research Laboratory at the University of Montana. An Omega DP24-T thermocouple meter was connected to the microscope objective using a glass-braided insulated thermocouple for determination of the sample temperature. Samples were excited with a vertically polarized 421 nm pulsed-diode laser (PicoQuant LDH-P-C-420) operating at a 3 μW average power (measured at the objective), and the vertical (V) and horizontal (H) components of the emission were collected on Hybrid-PMT detectors (PicoQuant). A 40 MHz repetition rate was used for the FCS measurements. Anisotropy measurements were collected at a 20 MHz repetition rate; V and H emission curves were collected for equal lengths of time, until 4×10^4 counts were obtained at the maximum of the V curve. High-density polyethylene glycol-coated coverslips (MicroSurfaces Inc.) were used for sample collection to avoid interaction of cyt*c* with the glass coverslip. A 30 μm pinhole and a 488 nm long-pass (LP) filter (AHF/Semrock BLP488-R) were used in the emission paths. A polarizing beam splitter (Ealing), placed behind the 488 LP filter, was used to separate the V- and H-polarized emission components for anisotropy measurements. The confocal volume was determined with Atto 425 dye in ultrapure water using a diffusion coefficient of 4.07×10^{-6} cm^2 s^{-1} at 25 °C.[66] SymPhoTime64 (PicoQuant version 2.3, build 4724) was used to collect data and analyze the FCS data. FluoFit (PicoQuant version 4.6.6.0, build 20.05.2014) was used to analyze the anisotropy data. Measurements were taken with monomeric and DSD human cyt*c* samples at ∼100 nM Zn-substituted heme (i.e., 100 nM monomer and 50 nM DSD). The titration procedure was the same as that used for CD titrations (1:1 mixing of Zncyt*c* and CL ND solutions at twice the desired final concentration). The anisotropy instrument response function (IRF) was obtained as described using Atto 425 quenched with a saturated aqueous KI solution.[67]

FCS data were fit using SymPhoTime64 version 2.3 (PicoQuant). Equation 4, which describes diffusion of several species in the presence of a single triplet state, was used as the fitting model. Figure S3 shows a typical FCS curve of Zncyt*c* binding to CL ND. A more complete treatment of the FCS equations that were used can be found in the Supporting Information.

$$G(t) = \left\{1 + T\left[\exp\left(-\frac{t}{\tau_T}\right) - 1\right]\right\} \times \sum_{i=0}^{n_{\text{D}}-1} \frac{\rho_i}{\left(1 + \frac{t}{\tau_{\text{D},i}}\right)\left(1 + \frac{t}{\tau_{\text{D},i}\kappa^2}\right)^{0.5}} \quad (4)$$

In eq 4, the first part of the equation in braces describes the triplet state, where T represents the fraction in the triplet (dark) state, τ_T is the time to relax from triplet back to the singlet state, and t is time. The second part of the equation describes the diffusion of molecules in the experiment. The contribution of the ith diffusing species is represented by ρ_i. $\tau_{\text{D},i}$ is the diffusion time of the ith species. κ is a geometrical factor describing the length:diameter ratio of the confocal volume.

Fluorescence anisotropy data were fit using the analysis software package FluoFit Pro version 4.6.6 (PicoQuant) according to the relationships described in eqs 5 and 6. A more complete treatment of the anisotropy equations used can be found in the Supporting Information.

$$I_{\text{VV}}(t) = (G_{\text{fac}})\text{IRF}_{\text{VV}}\frac{1}{3}\sum_{i=1}^{n}\alpha_i e^{-t/\tau_i}\left[1 + 2\left(R_{\text{INF}} + \sum_{j=1}^{n}\beta_j e^{-t/\phi_j}\right)\right] \quad (5)$$

$$I_{\text{VH}}(t) = \text{IRF}_{\text{VH}}\frac{1}{3}\sum_{i=1}^{n}\alpha_i e^{-t/\tau_i}\left[1 - \left(R_{\text{INF}} + \sum_{j=1}^{n}\beta_j e^{-t/\phi_j}\right)\right] \quad (6)$$

where G_{fac} is a weighting term that describes the transmission difference between the horizontal and vertical detection paths. The instrument response function (IRF) is used to deconvolute out the excitation pulse and detection electronics. τ_i is the lifetime and α_i the amplitude of the ith component in the intensity decay. R_{INF} is the anisotropy at infinite time or is due to a homogeneous, time-independent background.[68] The pre-exponential factors, β_j, represent the differences between the excitation and emission transition dipole moments of the probe and the symmetry axes of the protein.[69] The sum of β_j is the limiting anisotropy at time zero (r_0). The rotation correlation times, ϕ_j, are directly related to the size and shape of the protein as well as the temperature and viscosity of the aqueous solution.

All data were fit to one ϕ and an R_{INF}, where ϕ is that of the freely diffusing Zncyt*c*. Because the rotational correlation time of a Zncyt*c* bound to an ND is much longer than the fluorescence lifetime of Zncyt*c*, it is fit as R_{INF}; freely diffusing Zncyt*c* in the absence of NDs has an R_{INF} of 0. Figure S4 shows examples of fluorescence anisotropy decay curves.

Fitting Model for the Fluorescence Data. The FCS and anisotropy measurements are from experiments in which Zncyt*c* and CL ND are interacting at equilibrium (eq 7).

$$\text{Zncyt}c + \text{CL ND} \rightleftharpoons \text{Zncyt}c\cdots\text{CL ND} \quad (7)$$

The fractions bound (f_{bound}) or free (f_{free}) are directly calculated on the basis of the relative amplitudes of either their FCS diffusion coefficients or anisotropy rotational correlation times. In standard FCS measurements, it is

https://dx.doi.org/10.1021/acs.biochem.0c00326
Biochemistry XXXX, XXX, XXX−XXX

generally accepted that diffusion coefficients must differ by a factor of ~1.6−2 to be resolved.[70,71] A rough calculation using an estimate of the protein radius and the Stokes−Einstein relationship indicates that the monomer (~128 $\mu m^2/s$) or dimer (~101 $\mu m^2/s$) diffusion coefficients are larger by a factor of >2 than when bound to ND (~45 $\mu m^2/s$, estimated for 1:1 cytc−CL ND complexes), indicating that the free and bound species can be resolved. In anisotropy measurements, the interaction of Zncytc with the membrane surface of the ND will increase the rotational correlation time (ϕ), making it much longer than the fluorescence lifetime, resulting in a resolvable increase in R_{INF}.[72] Once f_{bound} has been determined, it can be directly plotted against the concentration of CL ND to obtain the association constant (K_a). The binding model is described by eq 8.

$$f_{bound} = \frac{[\text{Zncytc}\cdots\text{CL ND}]}{[\text{Zncytc}\cdots\text{CL ND}] + [\text{Zncytc}]} = \frac{K_a[\text{CL ND}]}{1 + K_a[\text{CL ND}]} \quad (8)$$

The native conformation of monomeric cytc is expected to require 9.1 nm^2 of membrane surface to bind.[73,74] A structural rearrangement upon binding could result in an increase in the requirement to ~13 nm^2.[73−75] The MSP1D1 NDs used in these experiments are expected to have a membrane surface area of ~72 nm^2 per side of the ND.[58] Thus, there is space for upward of five to eight molecules of cytc to bind per side of the ND assuming no repulsive interactions and ignoring entropy effects for binding on a continuous surface.[76] Under the conditions of our FCS experiments, the ND concentration is at least 100-fold higher than the cytc concentration near the midpoint of cytc−ND binding curves such that it is highly unlikely that more than one cytc will be bound per ND. Therefore, use of the non-interacting single-site binding equation given by eq 8 is a reasonable assumption to fit the FCS-monitored Cytc−ND binding data.

RESULTS AND DISCUSSION

Dissociation of the Human Cytc DSD to the Monomer Is Slow Compared to Those of Equine and Yeast DSDs. We have previously shown that the equine DSD is substantially more stable than the yeast WT* (K72A, C102S) iso-1-cytc dimer.[27] We hypothesized that if the DSD of cytc is involved in apoptosis, the evolution of the increased stability of the DSD could be an adaptation favoring more effective induction of the peroxidase activity of cytc as related to apoptosis in mammals. Our previous work[27] showed that the thermodynamic stability of monomeric cytc measured by guanidine hydrochloride (GdnHCl) unfolding[52] correlated well with the kinetic stability of the cytc DSD.

We have extended our studies of dimer dissociation kinetics to include the human cytc DSD, and we can now show that the human cytc DSD is even more stable than the equine cytc DSD, consistent with the great thermodynamic stability observed with GdnHCl unfolding of human cytc.[52] The Erying plot of the human DSD is compared to previously reported data for equine and yeast cytc in Figure 1. The human DSD was found to dissociate to the monomer at measurable rates in the same temperature range as the equine DSD (Table S1). It was kinetically more stable than the horse DSD of cytc with a lifetime that is longer by a factor of 2 (~2 weeks at 40 °C). All data in Figure 1 were fit to eq 1, which allows for curvature in the Eyring plot due to a change in heat capacity required to attain the transition state ($\Delta C_p^{\ddagger}$) for DSD dissociation.

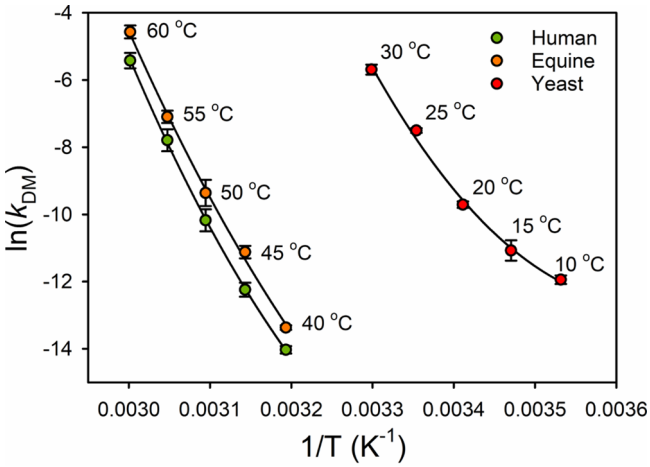

Figure 1. Eyring plots for dissociation of human WT (green), equine WT (orange), and yeast WT* (K72A, C102S mutations) (red) DSDs. The solid curve is a fit to a form of the Eyring equation that accounts for $\Delta C_p^{\ddagger}$ (eq 1). The reference temperature (T_0) was set to 310.15 K (37 °C) for all fits. The equine and yeast data are from ref 27.

Curvature in the plot indicates that $\Delta H_{T_0}^{\ddagger}$ and $\Delta S_{T_0}^{\ddagger}$ are both temperature-dependent.[77] We used the human physiological temperature (37 °C, 310.15 K) as the reference temperature, T_0, in the fits of the data in Figure 1 to eq 1 providing the activation parameters, $\Delta H_{T_0}^{\ddagger}$ and $\Delta S_{T_0}^{\ddagger}$ at 37 °C (Table 1). A large enthalpic barrier for spontaneous dissociation of the DSD to the monomer is observed for cytc of all three species.[27] However, favorable entropy compensates substantially for this large enthalpy, yielding a $\Delta G^{\ddagger}$ near 27 kcal/mol for the mammalian DSD compared to a value of ~19 kcal/mol for the yeast DSD at 37 °C. Plots of $\Delta G^{\ddagger}$ versus T, using the parameters in Table 1, show that the increased kinetic stability of the human DSD compared to that of the equine DSD arises from a shift in the temperature of maximum $\Delta G^{\ddagger}$ from 16 to 23 °C.

Table 1. Activation Parameters for Dissociation of Domain-Swapped Dimers to Monomers at 37 °C[a]

species	$\Delta H_{T_0}^{\ddagger}$ (kcal/mol)	$\Delta S_{T_0}^{\ddagger}$ (kcal mol^{-1} K^{-1})	$\Delta C_p^{\ddagger}$ (kcal mol^{-1} K^{-1})	$\Delta G^{\ddagger}$ (kcal/mol)
human	59 ± 4	0.10 ± 0.01	2.3 ± 0.3	27 ± 5
equine	66 ± 12	0.13 ± 0.04	1.8 ± 0.9	27 ± 16
yeast	107 ± 15	0.28 ± 0.05	3.1 ± 0.8	19 ± 21

[a]Data for yeast and equine cytc[27] were re-fit to eq 1 using a T_0 of 310.15 K. The error in $\Delta H_{T_0}^{\ddagger}$, $\Delta S_{T_0}^{\ddagger}$, and $\Delta C_p^{\ddagger}$ is the standard error of the parameter provided by SigmaPlot 13. The error in $\Delta G^{\ddagger}$ is the propagated error calculated from the error in $\Delta H_{T_0}^{\ddagger}$ and $\Delta S_{T_0}^{\ddagger}$.

Similar to the equine DSD,[27] the human DSD had less curvature in its Erying plot than the yeast DSD, yielding a $\Delta C_p^{\ddagger}$ smaller than that for the yeast DSD. All three values of $\Delta C_p^{\ddagger}$ indicate significant unfolding of both subunits during dissociation to the monomer because the ΔC_p values for thermal unfolding of the monomeric cytochromes c range from 1.1 to 1.4 kcal mol^{-1} K^{-1}.[47] The primary evolutionary adaptation that increases the kinetic stability of the DSD of mammalian versus yeast cytc is a decrease in $\Delta S_{T_0}^{\ddagger}$ at 37 °C. The larger $\Delta S_{T_0}^{\ddagger}$ for yeast DSD dissociation indicates that the TS is more disordered than the TS for dissociation of the

https://dx.doi.org/10.1021/acs.biochem.0c00326
Biochemistry XXXX, XXX, XXX−XXX

mammalian DSDs. The larger $\Delta C_p^{\ddagger}$ for the yeast versus the mammalian cyt*c* also is consistent with a larger degree of unfolding in the TS for the dimer-to-monomer dissociation of the yeast DSD.

For the FCS experiments described below, we use Zn-substituted monomeric and DSD human cyt*c*. The stability of Zn-substituted monomeric cyt*c* as measured by GdnHCl unfolding is similar to that of the native Fe protein.[78] Given the correlation between the kinetic stability of DSD cyt*c* and the stability of monomeric cyt*c* measured by GdnHCl unfolding discussed above, we expect the stability of the Zn-substituted human cyt*c* DSD to be similar to that measured for the Fe form of the human cyt*c* DSD.

The Alkaline Transition of the Human DSD Occurs 2.5 pH Units Lower Than That of the Monomer. It has been shown that a decrease in the midpoint pH ($pH_{1/2}$) of the alkaline transition can be correlated with better access to cyt*c* conformational states that promote peroxidase activity.[79−81] Below $pH_{1/2}$, Met80 is the predominate ligand bound to the heme, and above $pH_{1/2}$ Lys72, -73, and -79 from Ω-loop D are predominantly the bound ligands.[82] Lys binds more strongly to the Fe(III) of the heme than Met and is therefore a less labile ligand than Met80.[65] Thus, the lysine ligation of the alkaline state would be expected to decrease peroxidase activity. However, a decrease in the $pH_{1/2}$ of the alkaline transition correlates well with a decrease in the stability of Ω-loop D,[83,84] which protects the Met80 side of the heme.

Absorbance changes at 695 nm, an absorbance band that is present when Met80 is bound to the heme, were used to monitor the alkaline transition. A plot of $A_{695corr}$ versus pH in Figure 2 shows that the alkaline transition occurs at a much

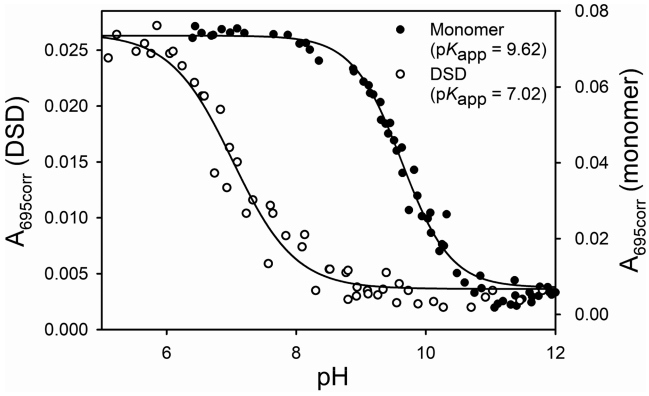

Figure 2. Plot of $A_{695corr}$ vs pH for the alkaline transition for monomeric (●) and DSD (○) cyt*c*. Data were collected at room temperature (22 ± 3 °C) in a 100 mM NaCl solution with a protein concentration of 100 μM heme (100 μM monomer or 50 μM DSD). Solids lines are fits to eq 2.

lower pH for the DSD than the monomer. The $pH_{1/2}$ we observe for the monomer (9.62 ± 0.03) is similar to the previously reported value.[52] By contrast, the $pH_{1/2}$ of the DSD (7.02 ± 0.06) is 2.5 pH units lower. The number of protons linked to the transition for both the monomer (1.15 ± 0.09) and the DSD (0.90 ± 0.11) was approximately equal to 1, which is consistent with a one-proton process, as normally observed for the alkaline transition of cyt*c*.[2,85]

Absorbance changes at 625 nm also provide information about dissociation of the Met80 ligand from the heme. An increase in A_{625} is observed below the $pH_{1/2}$ for the alkaline transition. This absorbance band has been attributed to formation of a high-spin heme state, resulting from a change in heme coordination to either a pentacoordinate state or a hexacoordinate state with a water molecule bound[86] in place of Met80. Whereas spectra of human DSD cyt*c*, acquired near pH 6, show a small peak near 625 nm (Figure S5), those of the monomeric human cyt*c* do not. Plots of $A_{625corr}$ versus pH show sigmoidal plots for both monomeric human cyt*c* and the DSD (Figure S6). For the DSD, the $pH_{1/2}$ is slightly lower than that of data monitored at 695 nm, indicating that Met80-heme and H_2O-heme ligation states are populating simultaneously as the pH is decreased below 7.

Taken together, these data indicate that the two hemes of the DSD are more accessible than the heme of the monomer. Met80, the primary ligand below $pH_{1/2}$, is located in the hinge-loop region of the dimer structure.[27,28] The population of an available coordination site, whether it is a pentacoordinate heme or a hexacoordinate heme with water bound, is larger for the DSD than for the monomer. The 2.5 pH unit decrease in the $pH_{1/2}$ of the DSD relative to that of the monomer places this change in ligation near physiological pH where it could directly regulate peroxidase activity *in vivo*.

Fluorescence Titrations Show That ND Binding by Human DSD Cyt*c* Is Weaker Than That of Monomeric Cyt*c*. Many studies of binding of cyt*c* to CL-containing liposomes involve titration of cyt*c*, at concentrations that are near the K_d, with increasing concentrations of CL typically in the form of liposomes.[75,87−90] Thus, accurate evaluation of K_d requires correction for bound CL. Estimates of the number of CL molecules bound to each cyt*c* cover a large range.[88,91] Direct experimental determination of the CL:cyt*c* stoichiometry has shown that this stoichiometry depends on ionic strength and requires prior experimental determination of the effective charge on the protein, *Z*, and an intrinsic binding constant, K_o, for the interaction from binding data as a function of salt concentration under low-binding conditions.[76] Because of the difficulty of accurately correcting for bound CL, it is often not done. To avoid this complication, we have used CL NDs as our model membrane system and FCS and fluorescence anisotropy as our detection methods. Using a fluorescent form of cyt*c*, Zncyt*c*, the concentration of monomeric and DSD cyt*c* can be kept between 50 and 100 nM, low enough that the total CL ND concentration does not need to be corrected for cyt*c*-bound CL ND. FCS reports on the translational diffusion of fluorescent species, while fluorescence anisotropy reports on rotational diffusion. These techniques are orthogonal methods for determining the hydrodynamic radius and therefore are complementary. The experimental setup used allows each individual sample to be measured by both methods; switching measurement modes requires only minor changes (e.g., changing the laser repetition rate and polarization of the fluorescence emission). This dual experimental approach provides an increased level of robustness to the results obtained.

The FCS curves for Zncyt*c* binding (Figure S3) were fit to two diffusion times (τ_D), a faster one representing a free species (free monomer or free DSD) and a slower one representing the ND-bound species, and a triplet state process (τ_T). The τ_D and translational diffusion coefficient (D) are related ($\tau_D = \omega_0^2/4D$) and can be connected to the hydrodynamic radius through the Stokes−Einstein equation; D is temperature- and viscosity-dependent, and τ_D depends on the size of the V_{eff}, which has been carefully calibrated. The

https://dx.doi.org/10.1021/acs.biochem.0c00326
Biochemistry XXXX, XXX, XXX−XXX

Table 2. Fluorescence Parameters for the Zncytc Monomer and DSD

	FCS				fluorescence anisotropy		
	τ_D (ms)	τ_T (μs)	D ($\mu m^2/s$)	R_H (nm)[a]	lifetime (ns)[b]	ϕ (ns)	R_H (nm)[a]
monomer	0.06 ± 0.01	12 ± 9	125 ± 21	1.80 ± 0.25	3.27 ± 0.31	6.37 ± 0.16	1.83 ± 0.05
monomer bound	0.48 ± 0.03	3 ± 2	33 ± 2.6	6.83 ± 0.51	–	–	–
DSD	0.08 ± 0.01	25 ± 5.2	92 ± 8.2	2.39 ± 0.19	4.55 ± 0.04	12.7 ± 0.17	2.31 ± 0.04
DSD bound	0.44 ± 0.02	2.7 ± 2.1	22 ± 2.4	10.1 ± 0.90	–	–	–

[a]R_H corrected to 25 °C from the experimental temperature. [b]The intensity-weighted lifetime is defined as $\langle\tau\rangle = \sum\alpha_i\tau_i^2/\sum\alpha_i\tau_i$.

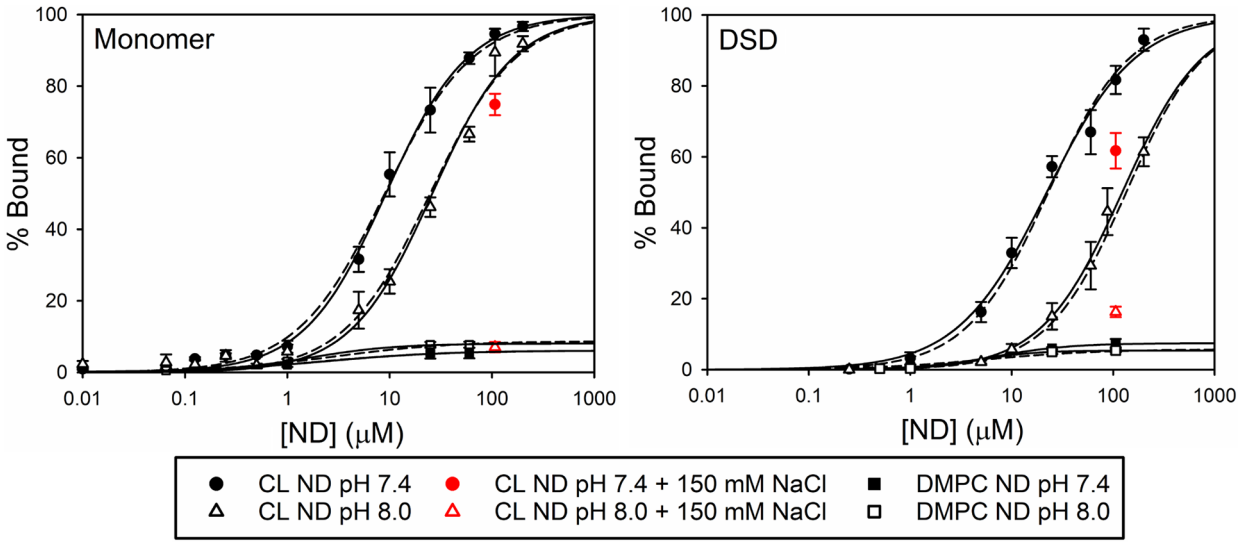

Figure 3. Plots of the percent bound monomeric (left) and DSD (right) Zncytc vs CL and DMPC nanodisc concentration (logarithmic scale) as determined by FCS and fluorescence anisotropy. Data points shown are from the FCS experiments. The fits of FCS (solid lines) and anisotropy (dashed lines) data sets to eq 8 are shown. Experimental data were corrected to 25 °C to determine binding, and experiments were performed in 20 mM TES at the indicated pH and salt concentration.

Table 3. Thermodynamic Parameters for Binding of Zncytc to CL ND from Fluorescence Experiments at 25 °C

		pH 7.4		pH 8.0	
		K_d (μM)	ΔG (kcal/mol)	K_d (μM)	ΔG (kcal/mol)
monomer	anisotropy	9.0 ± 0.2	6.88 ± 0.01	25 ± 0.6	6.28 ± 0.01
	FCS	9.2 ± 0.3	6.87 ± 0.02	26 ± 1.3	6.25 ± 0.03
DSD	anisotropy	23 ± 2	6.32 ± 0.05	134 ± 7.1	5.28 ± 0.03
	FCS	22 ± 1.2	6.35 ± 0.03	122 ± 6.0	5.34 ± 0.03

results are listed in Table 2. The free monomer and DSD diffusion coefficients are similar to the calculated values discussed in Materials and Methods. The experimental diffusion coefficients for cytc–ND complexes, however, are smaller than our calculated estimate in Materials and Methods (45 $\mu m^2/s$). Thus, the assumption of spherical symmetry may be inadequate for the CL ND complexes. The distinct difference in D for the monomer–ND complex versus the DSD–ND complex indicates that D is sensitive to the difference in size of the DSD versus monomeric forms of cytc bound to CL NDs.

The anisotropy decay data were fit to a single rotational correlation time ϕ (Table 2) with a limiting anisotropy (R_{INF}) because the ϕ of Zncytc bound to CL ND is much longer than the fluorescence lifetime and therefore difficult to fit with a second exponential. The binding can be followed, however, by the increase in R_{INF} and a decrease in the amplitude of the single ϕ as Zncytc binds to the CL NDs. Our parameters from analysis of the monomer fluorescence decay data (Table 2) agree well with those previously reported by Vanderkooi et al.[54] In addition, we observed a 1.3 ns increase in the intensity-weighted lifetime of the dimer compared with that of the monomer. The R_H values for the monomeric and DSD cytc extracted from the anisotropy data agree well with those obtained from FCS data (Table 2).

We carried out experiments at pH 8.0 and 7.4. At pH 8.0, we have shown that binding is dominated by site A (primarily electrostatic interaction) and appears to be weaker than for studies performed at lower pH values.[89] At pH ≤7.4,[92,93] binding is stronger and has a significant non-electrostatic component. Monomeric human cytc will be completely in the native state at both of these pH values. On the basis of the fit to the data in Figure 2, the human DSD will be 88% in the alkaline state at pH 8 and 69% in the alkaline state at pH 7.4. However, because of the high negative charge at the surface of the 100% CL NDs, the pH near the surface of the ND may be somewhat lower, which might lead to a larger shift toward population of the native conformer at pH 7.4. The data sets collected from FCS and fluorescence anisotropy measurements can be fit to a single-site binding model (eq 8). The fits to both

https://dx.doi.org/10.1021/acs.biochem.0c00326
Biochemistry XXXX, XXX, XXX–XXX

the FCS and anisotropy data can be seen in Figure 3. Binding constants extracted from these plots are listed in Table 3.

Control experiments (Figure 3) show that, regardless of pH, ~5% of the monomers and dimers of Zncyt*c* (100 nM Zn-heme concentration) bind to DMPC ND, which is likely nonspecific binding, perhaps to the belt protein.

We also measured the effect of adding NaCl to a final concentration of 150 mM to solutions containing Zncyt*c* fully bound to the CL NDs. At pH 8.0, when we added NaCl to the 100 μM CL ND titration point, the fraction of bound Zncyt*c* reverted to the level of binding observed with DMPC ND (Figure 3). This observation indicates that at pH 8.0, the cyt*c*−CL ND association is driven by electrostatic interaction at the A site. This result is consistent with our previous study of the binding of human and yeast cyt*c* to 100 nm CL liposomes, which indicated that the predominate binding interaction at pH 8 was through site A.[89] At pH 7.4, 150 mM salt causes only partial dissociation of cyt*c* from the CL ND. This behavior has previously been observed by other laboratories[43,87,88] and indicates that at pH 7.4 binding sites on cyt*c* that have a significant hydrophobic component also contribute to binding.

The binding data for the Zncyt*c* monomer (Figure 3, Figure S7, and Table 3) also show that increasing the pH from 7.4 to 8.0 results in a 2-fold increase in the K_d. This result is consistent with the weaker influence of binding sites other than the A site at pH 8, as indicated by the weaker effect of 150 mM salt on binding at pH 7.4 versus pH 8.0. These results fit with previously published binding data,[89,90,94] and they support the interpretation that multiple cyt*c* binding sites are involved in the interaction with CL surfaces. These data also support previous data, which suggest that at lower pH values multiple binding locations on cyt*c* work in concert to form a tighter interaction[91,95] that then may be followed by a second unfolding stage.[43,88,92] These observations could also indicate that the combined effects of these binding sites at lower pH either result from an overly strong electrostatic interaction to be broken at the NaCl levels used in this experiment or rely on hydrophobic interactions usually associated with the C site.

The dimer binding data (Table 3) show a decrease in the affinity for a CL surface: the K_d of the dimer at pH 7.4 is similar to that of the monomer at pH 8.0, and there is a 5-fold decrease in the binding affinity of the dimer when the pH is increased from 7.4 to 8.0. This decrease in affinity at pH 8 indicates that the A site of the dimer makes a weaker contribution to the cyt*c*−CL interaction under these conditions. Thus, formation of the dimer reduces the binding interaction with the CL surface, which could indicate another way in which the dimer has evolved into a dynamic switch to control apoptosis near physiological pH. The decrease in affinity at higher pH may be linked to the alkaline conformational transition of the dimer because the population of this conformer is somewhat higher at pH 8 than at pH 7.4.

The significantly different diffusion coefficients observed for CL ND-bound monomeric cyt*c* versus CL ND-bound DSD cyt*c* (Table 2) and the considerably different K_d values observed for the monomer and DSD cyt*c* binding to CL NDs (Figure 3 and Table 3) suggest that human DSD cyt*c* does not dissociate to the monomer when bound to CL NDs. These observations are consistent with the high stability of human DSD cyt*c* (Figure 1 and Table 1). However, further experiments would be required to demonstrate definitively that human DSD cyt*c* binding to CL NDs does not cause any dissociation of the DSD to the monomer.

CD Binding Experiments Show Cooperative Binding with an Increased Concentration of Cytc. It has been shown that ruffling, the perturbation of the heme from perfect D_{4h} symmetry, is influenced by the CXXCH heme attachment sequence and the residues that pack against this sequence.[96−98] Breaking of this symmetry leads to a strong circular dichroism (CD) signal in the Soret region.[99] The amplitude of the B-band couplet in the Soret CD is dependent on both the splitting of the band and the rotational strength.[100] Coupling of the heme $\pi-\pi^*$ transitions to those of nearby aromatic amino acids is believed to be an important mechanism for induction of rotational strength.[101] Mutagenesis studies with yeast iso-1-cyt*c* implicate Phe82, which packs against the heme, as an important contributor to the Soret CD of cyt*c*.[102] Thus, local rearrangement of the heme environment can significantly affect the Soret CD. Changes in the CD spectrum have been used successfully to study the rearrangement of the heme environment of cyt*c* that occurs when the protein binds to liposomes.[33,88,89,92,103−106]

The human monomer and DSD cyt*c* have markedly different signatures in the Soret CD spectra at pH 8.0 (Figure 4). The

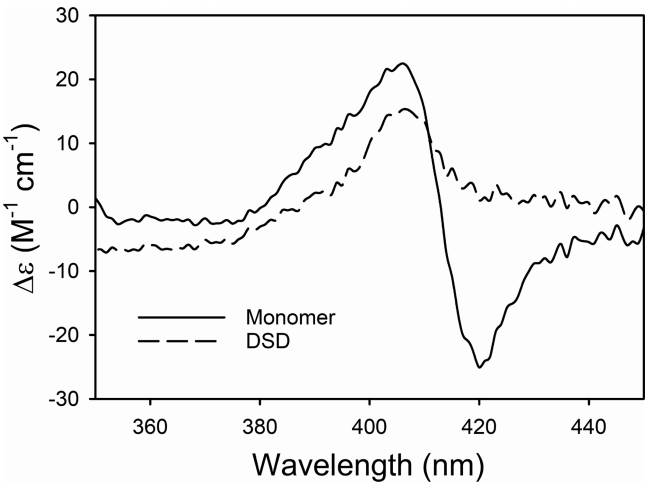

Figure 4. Soret CD spectra of human monomer (solid line) and DSD (dashed line) cyt*c* at a heme concentration of 10 μM (10 μM monomer or 5 μM DSD). Spectra were recorded in 20 mM TES buffer and 0.1 mM EDTA (pH 8.0) at 25 °C.

degree of B-band splitting reported here for the monomer is similar to that reported in previous studies.[89] The lack of a trough in the DSD spectrum is only seen for the monomer at high lipid:cyt*c* ratios, where it indicates a significant perturbation of the heme environment of the monomer.[89] The dimer CD spectra are similar to those previously reported for the equine alkaline conformation,[107] suggesting that the human dimer is in an alkaline conformation at pH 8. The data in Figure 2 support this conclusion.

The Soret CD spectrum from 350 to 450 nm was monitored as CL NDs were titrated against a fixed concentration of monomeric and DSD human cyt*c* at pH 8, where the electrostatic site A binding site dominates binding.[89] On the basis of the FCS data, the CD experiments were performed at protein concentrations close to the K_d of the monomer but well below that of the DSD. The CD experiments were performed at a concentration of cyt*c* 100-fold higher than that in the fluorescence experiments. Because of the small surface area of the ND, the higher concentrations of cyt*c* used in the

https://dx.doi.org/10.1021/acs.biochem.0c00326
Biochemistry XXXX, XXX, XXX−XXX

CD experiments could result in crowding that would lead to interactions between individual cyt*c* molecules on the surface of the ND, potentially increasing the apparent affinity of the ND for monomer or DSD forms of cyt*c*.

When titrated against CL ND, the Soret CD signals of the monomer and DSD respond differently at pH 8 (Figure S8). Qualitative binding of the monomer differs with respect to binding to liposomes, too.[89] When the monomer binds to 100% CL liposomes, there is a strong increase in the amplitude of the 405 nm peak, followed by a red shift of the peak as the trough near 418 nm disappears.[89] Unlike the liposome binding data, there is a decrease in the amplitude of the 405 nm peak with the addition of ND. The largest change in the monomer Soret CD spectrum is the decrease in the amplitude of the 418 nm trough as the CL ND concentration increases. For the DSD, there is only a small increase in the intensity of the Soret CD band centered at 410 nm.

Data at these wavelengths are plotted versus ND concentration in Figure 5. We use a single-site Langmuir-type binding isotherm (eq S14 in the Supporting Information) to fit these data, as previously described.[89] As shown in Table 4, the K_d(app) obtained from the Soret CD data indicates binding that is tighter than that of the fluorescence data (Table 3). This observation could suggest that interactions between human cyt*c* molecules increase the affinity for CL NDs under crowded conditions (higher cyt*c* concentration coupled to low ND:cyt*c* ratios). The 100-fold higher Cyt*c* concentration leads to an ~10-fold decrease in the K_d(app) for monomeric cyt*c* and a >100-fold decrease for the DSD. For the DSD, there is likely a significant error in K_d(app) because of the low amplitude of the signal change caused by binding to the CL NDs. At the midpoint of the titration of the CL NDs by the DSD, ~8 DSDs would be bound per ND. Assuming the dimer requires twice the surface area of the monomer, essentially all of the available space on both sides of the ND would be occupied [8 monomers can fit on the surface of each side of an ND (see Materials and Methods)]. While entropy effects might be expected to oppose such high occupancy,[76] entropy could be mitigated by interaction between dimers. For monomeric horse cyt*c* binding to phosphatidylglycerol (PG), ligand−ligand interaction was observed to be negligible.[76] However, for denatured horse cyt*c* binding to PG, significant ligand−ligand interaction was observed.[76] Thus, it is possible that the dimer behaves more like denatured cyt*c* in this regard. Data for the horse cyt*c* dimer binding to PG-containing liposomes also show that the dimer binds more tightly than the monomer when the cyt*c* concentration is in the micromolar range.[108] The cooperativity parameter, *n*, is near 1 for both the monomer and the dimer (Table 4). We are varying the ND concentration, so the value of *n* suggests that there is no cooperativity with respect to the ND [or CL (Figure S9)].

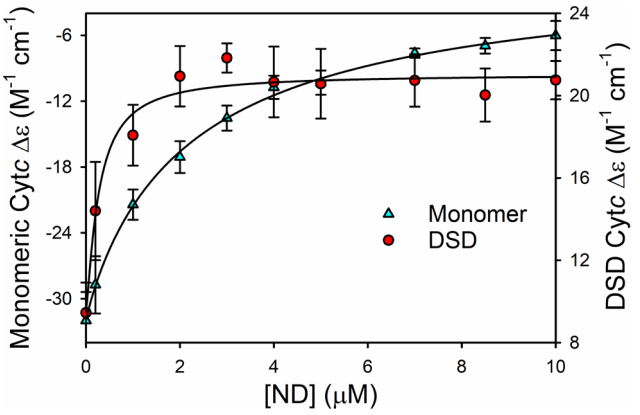

Figure 5. Human cyt*c* Soret CD signal as a function of the concentration of cardiolipin ND, [ND]. Data points at each [ND] follow the change in amplitude of the peak of the Soret CD signal. For the monomer the changes at 418 nm and for the DSD the changes at 410 nm are plotted vs [ND]. The experimental concentration of cyt*c* was 10 μM based on the heme absorbance (i.e., 10 μM monomer or 5 μM DSD). Experiments were performed in 20 mM TES buffer and 0.1 mM EDTA (pH 8) at 25 °C. Solid curves are fits to eq S14 in the Supporting Information.

Table 4. Thermodynamic Parameters for Binding of Cyt*c* to CL NDs from CD Data at 25 °C and pH 8

variant	K_d(app) (μM ND)[a]	*n*
monomer−ND	2.3 ± 0.1	0.9 ± 0.3
DSD−ND	0.3 ± 0.1	1.2 ± 0.4

[a]The experimental concentration of cyt*c* was 10 μM based on the heme absorbance (i.e., 10 μM monomer or 5 μM DSD). The error corresponds to the standard error in the fit of the parameter. We use the apparent dissociation constant, K_d(app), because we have not corrected the ND concentration for ND bound to cyt*c*.

For the monomer, on average ~2 monomers would be bound per ND at the midpoint (one per side). This observation indicates that ligand−ligand interaction is less significant for monomeric cyt*c* compared to the dimer, consistent with previous work.[76] When the response of the CD signal is plotted versus the lipid:protein ratio, the binding curves for CL NDs and CL liposomes are identical for the cyt*c* monomer (Figure S9). Therefore, the effect of cyt*c* concentration on K_d(app) cannot be attributed to a difference between NDs and liposomes.

At the K_d measured by single-molecule fluorescence methods at pH 8 (Table 3), the ND:cyt*c* ratio is ~100 for the monomer and >1000 for the DSD, so it is unlikely that more than one cyt*c* monomer or dimer is bound to each ND. Under conditions of high protein dilution with respect to ND concentration, effects of ligand−ligand interaction would be expected to be minimal.

The Human Cyt*c* DSD Shows Increased Peroxidase Activity in the Absence and Presence of CL NDs. As previously discussed, cyt*c*'s ability to become a peroxidase is essential for its role as an initiator of the intrinsic apoptotic pathway.[10,109] Increasing the flexibility of Ω-loop D or the removal of the heme ligand provided by Ω-loop D has been shown to increase peroxidase activity in monomeric cyt*c*.[110,111] In the DSD conformation, Ω-loop D is conformationally distant from the heme and the Met80 ligand is replaced with H_2O,[27,28] which should result in an increase in peroxidase activity, as has been shown for the equine DSD of cyt*c* in aqueous solution at pH 7.[44] To determine the effect of formation of the alkaline conformer of the DSD on peroxidase activity, we have measured its peroxidase activity from pH 6 to 8. To evaluate the peroxidase activity of monomeric and DSD human cyt*c* bound to NDs though site A, we performed experiments in the presence and absence of CL NDs at pH 8.[89]

Michaelis−Menten plots of peroxidase activity were generated from data obtained by monitoring the formation of tetraguaiacol from guaiacol at 470 nm in the presence of H_2O_2. These plots were used to determine the catalytic rate

https://dx.doi.org/10.1021/acs.biochem.0c00326
Biochemistry XXXX, XXX, XXX−XXX

Table 5. Peroxidase Activity of Human Cytc Variants as a Function of pH at 25 °C with Guaiacol as the Substrate

	pH 6.0		pH 7.0		pH 8.0	
variant	K_m (M)	k_{cat} (s^{-1})	K_m (M)	k_{cat} (s^{-1})	K_m (M)	k_{cat} (s^{-1})
monomer[a]	14 ± 2	0.11 ± 0.01	5.7 ± 0.3	0.11 ± 0.002	11 ± 2	0.06 ± 0.01
monomer with CL ND[b]					6 ± 3	0.29 ± 0.03
					11 ± 2	0.06 ± 0.01
DSD	11 ± 1	1.52 ± 0.02	12 ± 3	0.78 ± 0.04	18 ± 3	0.44 ± 0.02
DSD with CL ND					24 ± 6	1.43 ± 0.12

[a]Parameters are from ref 101. [b]Samples with CL ND led to a biphasic data set.

constant (k_{cat}) and the Michaelis–Menten constant (K_m) for cytc. The data were normalized on the basis of the amount of heme present (i.e., the concentration of DSD is half that of the monomer). Figure S10 shows Michaelis–Menten plots generated from peroxidase data acquired for the monomer and DSD, with and without CL ND at pH 8.0. While the K_m values are relatively similar (also see Table 5), the k_{cat} values increase from the monomer to the DSD. The k_{cat} values also increase dramatically in the presence of CL NDs.

The data in Table 5 show that k_{cat} decreases as the pH increases for both monomeric and DSD human cytc. A decrease in k_{cat} as the pH increases has been observed for both horse and human monomeric cytc.[65,110,112] This trend has been attributed to replacement of Met80 with lysine[65] because nitrogen donors are much stronger ligands for Fe(III)heme than methionine.[113,114] For the DSD of human cytc, k_{cat} decreases smoothly (Figure 6, left panel) as the DSD forms

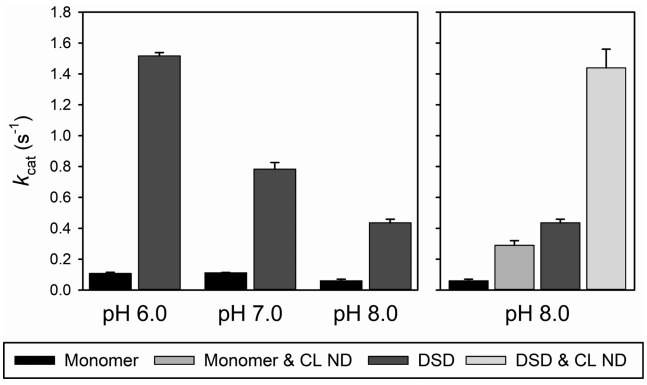

Figure 6. k_{cat} vs pH for monomeric and DSD cytc at 25 °C. Error bars are the standard deviations from three independent experiments. Human data in the absence of CL NDs are from ref 102.

an alkaline state ($pH_{1/2}$ = 7.02 ± 0.06). Thus, the peroxidase activity of the DSD can function as a pH-inducible switch near physiological pH. Also, the peroxidase activity of the human DSD is 7-fold higher than that of the monomer at pH 7 and 8 but 14-fold higher at pH 6 when mixed Met80/H_2O ligation replaces the lysine ligation of the alkaline state (see Figure 2 and Figures S5 and S6).

The initial velocity (v) was determined by finding the greatest slope in the A_{470} versus time data after an initial lag. At pH 8, the monomer cytc data in the presence of CL NDs presented a curve with a second obvious slope before approaching saturation, indicating the presence of at least two catalytically distinct species. Both of these velocities were used to determine a K_m and a k_{cat}. One set of Michaelis–Menten parameters showed a larger k_{cat} (0.29 ± 0.01 s^{-1}) and a smaller K_m (6 ± 3 μM) compared to those observed for the monomer in the absence of NDs (see Table 5, Figure 6, and Figure S10). The other set of parameters matched that of free monomeric cytc in solution (see Table 5). The observation of two kinetic phases under the conditions of peroxidase activity measurements (1 μM cytc and 1 μM ND) is consistent with the binding curve in Figure 5, which indicates that monomeric cytc would not be fully bound to the NDs under these conditions. The k_{cat} for the ND bound monomer is based on the total concentration of the monomer and thus may be an underestimate.

The unfolding of cytc by guanidine hydrochloride has been shown to increase the peroxidase activity to rates similar to those observed for isolated heme groups.[115] Likewise, the addition of CL membrane mimics has been shown to result in a dramatic increase in the peroxidase activity of monomeric cytc.[59] Our data are consistent with these observations, with the DSD showing increased peroxidase activity over the monomer, and the peroxidase activity of both species increasing in the presence of CL NDs at pH 8 when bound through site A.

CONCLUSIONS

The data presented provide evidence for how the DSD conformer of cytc may be an evolved switch to allow tighter control of the intrinsic apoptotic pathway. The human cytc DSD is substantially more stable to dissociation than that of yeast. Because yeast lacks a complete apoptotic pathway,[116] the increased stability of human and equine cytc DSDs could indicate evolution in mammals to regulate the intrinsic apoptotic pathway. The DSD of human cytc undergoes an alkaline conformational transition with a midpoint near neutral pH. The structural reorganization seems to act as a conformational switch that increases the affinity for CL NDs by 5-fold from pH 8 to 7.4 and also leads to a progressive increase in peroxidase activity as the pH is decreased from 8 to 6. The alkaline conformer of the DSD converts to a mix of Met80-ligated and high-spin (H_2O-ligated) heme by pH 6, leading to a larger enhancement in peroxidase activity as the pH decreases from 8 to 6 compared to that of monomeric human cytc. The DSD of human cytc is well-adapted to act as a pH-sensitive functional switch near the pH of the IMS (pH 6.88 ± 0.08).[117] During apoptosis, the pH of the cytoplasm decreases below 6.[118] If the same were true of the IMS, the intrinsic peroxidase activity of the DSD would continue to increase (Figure 6).

Our results also suggest that self-interaction between cytc molecules may enhance the affinity of cytc for CL-containing membranes under crowded conditions. DSD affinity appears to be more strongly enhanced than that of the monomer. This effect of cytc concentration on the strength of the interaction

https://dx.doi.org/10.1021/acs.biochem.0c00326
Biochemistry XXXX, XXX, XXX–XXX

of cytc with CL membranes bears further investigation given the millimolar concentration of cytc in mitochondria.[119,120]

■ ASSOCIATED CONTENT

Supporting Information

The Supporting Information is available free of charge at https://pubs.acs.org/doi/10.1021/acs.biochem.0c00326.

A more detailed derivation of the equations used to fit single-molecule fluorescence data, figures showing the structure of one subunit of the cytc DSD, the intermediates in the production of zinc-substituted cytc, a typical FCS correlation function plot for cytc−ND binding, typical fluorescence anisotropy data, spectra showing the 695 and 625 nm bands as a function of pH for monomeric and DSD cytc, a plot of absorbance at 625 nm versus pH for monomeric and DSD human WT cytc, binding curves for the interaction of monomeric and DSD cytc with CL NDs, CD spectra as a function of CL ND concentration, and Michaelis−Menten plots for monomeric and DSD cytc in the presence and absence of CL NDs at pH 8, and a table containing the k_{DM} values for the human DSD used in Figure 1 (PDF)

Accession Codes

UniProt ID of human cytochrome *c*, P99999.

■ AUTHOR INFORMATION

Corresponding Author

Bruce E. Bowler − *Department of Chemistry & Biochemistry and Center for Biomolecular Structure & Dynamics, University of Montana, Missoula, Montana 59812, United States;* orcid.org/0000-0003-1543-2466; Phone: (406) 243-6114; Email: bruce.bowler@umontana.edu; Fax: (406) 243-4227

Authors

Harmen B. B. Steele − *Department of Chemistry & Biochemistry and Center for Biomolecular Structure & Dynamics, University of Montana, Missoula, Montana 59812, United States*

Margaret M. Elmer-Dixon − *Department of Chemistry & Biochemistry and Center for Biomolecular Structure & Dynamics, University of Montana, Missoula, Montana 59812, United States*

James T. Rogan − *Department of Chemistry & Biochemistry, University of Montana, Missoula, Montana 59812, United States*

J. B. Alexander Ross − *Department of Chemistry & Biochemistry and Center for Biomolecular Structure & Dynamics, University of Montana, Missoula, Montana 59812, United States*

Complete contact information is available at: https://pubs.acs.org/10.1021/acs.biochem.0c00326

Funding

This work was supported by grants from the National Science Foundation [CHE-1609720 and CHE-1904895 (B.E.B.)]. The BioSpectroscopy Core Research Laboratory at the University of Montana was supported by a CoBRE grant from the National Institute of General Medical Sciences (P20GM103546).

Notes

The authors declare no competing financial interest.

■ ABBREVIATIONS

IMS, intermembrane space; CL, cardiolipin; DSD, domain-swapped dimer; CD, circular dichroism; FCS, fluorescence correlation spectroscopy; cytc, cytochrome *c*; Zncytc, zinc-substituted cytc; ND, nanodisc; DMPC, 1,2-dimyristoyl-*sn*-glycero-3-phosphocholine; k_{DM}, rate constant for conversion of the DSD to the monomer; GdnHCl, guanidine hydrochloride.

■ REFERENCES

(1) Dickerson, R. E., and Timkovich, R. (1975) Cytochromes *c*. In *The Enzymes* (Boyer, P. D., Ed.) 3rd ed., pp 397−547, Academic Press, New York.

(2) Moore, G. R., and Pettigrew, G. W. (1990) *Cytochromes c: Evolutionary, Structural and Physicochemical Aspects*, Springer-Verlag, New York.

(3) Winge, D. R. (2012) Sealing the mitochondrial respirasome. *Mol. Cell. Biol. 32*, 2647−2652.

(4) Berghuis, A. M., and Brayer, G. D. (1992) Oxidation state-dependent conformational changes in cytochrome *c*. *J. Mol. Biol. 223*, 959−976.

(5) Deacon, O. M., Karsisiotis, A. I., Moreno-Chicano, T., Hough, M. A., Macdonald, C., Blumenschein, T. M. A., Wilson, M. T., Moore, G. R., and Worrall, J. A. R. (2017) Heightened dynamics of the oxidized Y48H variant of human cytochrome *c* increases its peroxidatic activity. *Biochemistry 56*, 6111−6124.

(6) Liu, X., Kim, C. N., Yang, J., Jemmerson, R., and Wang, X. (1996) Induction of apoptotic program in cell-free extracts: requirement for dATP and cytochrome *c*. *Cell 86*, 147−157.

(7) Fulda, S., and Debatin, K. M. (2006) Extrinsic versus intrinsic apoptosis pathways in anticancer chemotherapy. *Oncogene 25*, 4798−4811.

(8) van Loo, G., Saelens, X., van Gurp, M., MacFarlane, M., Martin, S. J., and Vandenabeele, P. (2002) The role of mitochondrial factors in apoptosis: a Russian roulette with more than one bullet. *Cell Death Differ. 9*, 1031−1042.

(9) Huberts, D. H. E. W., and van der Klei, I. J. (2010) Moonlighting proteins: an intriguing mode of multitasking. *Biochim. Biophys. Acta, Mol. Cell Res. 1803*, 520−525.

(10) Jiang, X., and Wang, X. (2004) Cytochrome *c*-mediated apoptosis. *Annu. Rev. Biochem. 73*, 87−106.

(11) Orrenius, S., and Zhivotovsky, B. (2005) Cardiolipin oxidation sets cytochrome *c* free. *Nat. Chem. Biol. 1*, 188−189.

(12) Kagan, V. E., Tyurin, V. A., Jiang, J., Tyurina, Y. Y., Ritov, V. B., Amoscato, A. A., Osipov, A. N., Belikova, N. A., Kapralov, A. A., Kini, V., Vlasova, I. I., Zhao, Q., Zou, M., Di, P., Svistunenko, D. A., Kurnikov, I. V., and Borisenko, G. G. (2005) Cytochrome *c* acts as a cardiolipin oxygenase required for release of proapoptotic factors. *Nat. Chem. Biol. 1*, 223−232.

(13) Kagan, V. E., Borisenko, G. G., Tyurina, Y. Y., Tyurin, V. A., Jiang, J., Potapovich, A. I., Kini, V., Amoscato, A. A., and Fujii, Y. (2004) Oxidative lipidomics of apoptosis: redox catalytic interactions of cytochrome *c* with cardiolipin and phosphatidylserine. *Free Radical Biol. Med. 37*, 1963−1985.

(14) Ott, M., Robertson, J. D., Gogvadze, V., Zhivotovsky, B., and Orrenius, S. (2002) Cytochrome *c* release from mitochondria proceeds by a two-step process. *Proc. Natl. Acad. Sci. U. S. A. 99*, 1259.

(15) Shidoji, Y., Hayashi, K., Komura, S., Ohishi, N., and Yagi, K. (1999) Loss of molecular interaction between cytochrome *c* and cardiolipin due to lipid peroxidation. *Biochem. Biophys. Res. Commun. 264*, 343−347.

(16) Kagan, V. E., Tyurina, Y. Y., Bayir, H., Chu, C. T., Kapralov, A. A., Vlasova, I. I., Belikova, N. A., Tyurin, V. A., Amoscato, A., Epperly, M., Greenberger, J., DeKosky, S., Shvedova, A. A., and Jiang, J. (2006) The "pro-apoptotic genies" get out of mitochondria: oxidative

https://dx.doi.org/10.1021/acs.biochem.0c00326
Biochemistry XXXX, XXX, XXX−XXX

lipidomics and redox activity of cytochrome *c*/cardiolipin complexes. *Chem.-Biol. Interact. 163*, 15−28.
(17) McMillin, J. B., and Dowhan, W. (2002) Cardiolipin and apoptosis. *Biochim. Biophys. Acta, Mol. Cell Biol. Lipids 1585*, 97−107.
(18) Horvath, S. E., and Daum, G. (2013) Lipids of mitochondria. *Prog. Lipid Res. 52*, 590−614.
(19) Nicholls, P. (1974) Cytochrome *c* binding to enzymes and membranes. *Biochim. Biophys. Acta, Rev. Bioenerg. 346*, 261−310.
(20) Scorrano, L., Ashiya, M., Buttle, K., Weiler, S., Oakes, S. A., Mannella, C. A., and Korsmeyer, S. J. (2002) A distinct pathway remodels mitochondrial cristae and mobilizes cytochrome *c* during apoptosis. *Dev. Cell 2*, 55−67.
(21) Montero, J., Mari, M., Colell, A., Morales, A., Basañez, G., Garcia-Ruiz, C., and Fernández-Checa, J. C. (2010) Cholesterol and peroxidized cardiolipin in mitochondrial membrane properties, permeabilization and cell death. *Biochim. Biophys. Acta, Bioenerg. 1797*, 1217−1224.
(22) Eckmann, J., Eckert, S. H., Leuner, K., Muller, W. E., and Eckert, G. P. (2013) Mitochondria: mitochondrial membranes in brain ageing and neurodegeneration. *Int. J. Biochem. Cell Biol. 45*, 76−80.
(23) Fernandez, M. G., Troiano, L., Moretti, L., Nasi, M., Pinti, M., Salvioli, S., Dobrucki, J., and Cossarizza, A. (2002) Early changes in intramitochondrial cardiolipin distribution during apoptosis. *Cell Growth Differ. 13*, 449−455.
(24) Gonzalvez, F., and Gottlieb, E. (2007) Cardiolipin: setting the beat of apoptosis. *Apoptosis 12*, 877−885.
(25) Epand, R. F., Martinou, J. C., Fornallaz-Mulhauser, M., Hughes, D. W., and Epand, R. M. (2002) The apoptotic protein tBid promotes leakage by altering membrane curvature. *J. Biol. Chem. 277*, 32632−32639.
(26) Gronenborn, A. M. (2009) Protein acrobatics in pairs - dimerization via domain swapping. *Curr. Opin. Struct. Biol. 19*, 39−49.
(27) McClelland, L. J., Steele, H. B. B., Whitby, F. G., Mou, T.-C., Holley, D., Ross, J. B. A., Sprang, S. R., and Bowler, B. E. (2016) Cytochrome *c* can form a well-defined binding pocket for hydrocarbons. *J. Am. Chem. Soc. 138*, 16770−16778.
(28) Hirota, S., Hattori, Y., Nagao, S., Taketa, M., Komori, H., Kamikubo, H., Wang, Z., Takahashi, I., Negi, S., Sugiura, Y., Kataoka, M., and Higuchi, Y. (2010) Cytochrome *c* polymerization by successive domain swapping at the C-terminal helix. *Proc. Natl. Acad. Sci. U. S. A. 107*, 12854−12859.
(29) Fetrow, J. S., Dreher, U., Wiland, D. J., Schaak, D. L., and Boose, T. L. (1998) Mutagenesis of histidine 26 demonstrates the importance of loop-loop and loop-protein interactions for the function of iso-1-cytochrome *c*. *Protein Sci. 7*, 994−1005.
(30) McClelland, L. J., Mou, T.-C., Jeakins-Cooley, M. E., Sprang, S. R., and Bowler, B. E. (2014) Structure of a mitochondrial cytochrome *c* conformer competent for peroxidase activity. *Proc. Natl. Acad. Sci. U. S. A. 111*, 6648−6653.
(31) Rytömaa, M., and Kinnunen, P. K. J. (1994) Evidence for two distinct acidic phospholipid-binding sites in cytochrome *c*. *J. Biol. Chem. 269*, 1770−1774.
(32) Kooijman, E. E., Swim, L. A., Graber, Z. T., Tyurina, Y. Y., Bayır, H., and Kagan, V. E. (2017) Magic angle spinning ^{31}P NMR spectroscopy reveals two essentially identical ionization states for the cardiolipin phosphates in phospholipid liposomes. *Biochim. Biophys. Acta, Biomembr. 1859*, 61−68.
(33) Malyshka, D., Pandiscia, L. A., and Schweitzer-Stenner, R. (2014) Cardiolipin containing liposomes are fully ionized at physiological pH. An FT-IR study of phosphate group ionization. *Vib. Spectrosc. 75*, 86−92.
(34) Houtkooper, R. H., and Vaz, F. M. (2008) Cardiolipin, the heart of mitochondrial metabolism. *Cell. Mol. Life Sci. 65*, 2493−2506.
(35) Hayashi, Y., Yamanaka, M., Nagao, S., Komori, H., Higuchi, Y., and Hirota, S. (2016) Domain swapping oligomerization of thermostable *c*-type cytochrome in *E. coli* cells. *Sci. Rep. 6*, 19334.
(36) Lin, T.-Y., and Weibel, D. B. (2016) Organization and function of anionic phospholipids in bacteria. *Appl. Microbiol. Biotechnol. 100*, 4255−4267.
(37) Yang, H., Yamanaka, M., Nagao, S., Yasuhara, K., Shibata, N., Higuchi, Y., and Hirota, S. (2019) Protein surface charge effect on 3D domain swapping in cells for *c*-type cytochromes. *Biochim. Biophys. Acta, Proteins Proteomics 1867*, 140265.
(38) Hayashi, Y., Nagao, S., Osuka, H., Komori, H., Higuchi, Y., and Hirota, S. (2012) Domain swapping of the heme and N-terminal α-helix in *Hydrogenobacter thermophilus* cytochrome c_{552} dimer. *Biochemistry 51*, 8608−8616.
(39) Yamanaka, M., Nagao, S., Komori, H., Higuchi, Y., and Hirota, S. (2015) Change in structure and ligand binding properties of hyperstable cytochrome c_{555} from *Aquifex aeolicus* by domain swapping. *Protein Sci. 24*, 366−375.
(40) Nagao, S., Ueda, M., Osuka, H., Komori, H., Kamikubo, H., Kataoka, M., Higuchi, Y., and Hirota, S. (2015) Domain-swapped dimer of *Pseudomonas aeruginosa* cytochrome c_{551}: structural insights into domain swapping of cytochrome *c* family proteins. *PLoS One 10*, e0123653.
(41) Parui, P. P., Deshpande, M. S., Nagao, S., Kamikubo, H., Komori, H., Higuchi, Y., Kataoka, M., and Hirota, S. (2013) Formation of oligomeric cytochrome *c* during folding by intermolecular hydrophobic interaction between N- and C-terminal α-helices. *Biochemistry 52*, 8732−8744.
(42) Maity, H., Maity, M., Krishna, M. M., Mayne, L., and Englander, S. W. (2005) Protein folding: the stepwise assembly of foldon units. *Proc. Natl. Acad. Sci. U. S. A. 102*, 4741−4746.
(43) Hanske, J., Toffey, J. R., Morenz, A. M., Bonilla, A. J., Schiavoni, K. H., and Pletneva, E. V. (2012) Conformational properties of cardiolipin-bound cytochrome *c*. *Proc. Natl. Acad. Sci. U. S. A. 109*, 125−130.
(44) Wang, Z., Matsuo, T., Nagao, S., and Hirota, S. (2011) Peroxidase activity enhancement of horse cytochrome *c* by dimerization. *Org. Biomol. Chem. 9*, 4766−4769.
(45) Dawson, J. H. (1988) Probing structure-function relations in heme-containing oxygenases and peroxidases. *Science 240*, 433.
(46) Hersleth, H.-P., Ryde, U., Rydberg, P., Görbitz, C. H., and Andersson, K. K. (2006) Structures of the high-valent metal-ion haem−oxygen intermediates in peroxidases, oxygenases and catalases. *J. Inorg. Biochem. 100*, 460−476.
(47) Olteanu, A., Patel, C. N., Dedmon, M. M., Kennedy, S., Linhoff, M. W., Minder, C. M., Potts, P. R., Deshmukh, M., and Pielak, G. J. (2003) Stability and apoptotic activity of recombinant human cytochrome *c*. *Biochem. Biophys. Res. Commun. 312*, 733−740.
(48) Duncan, M. G., Williams, M. D., and Bowler, B. E. (2009) Compressing the free energy range of substructure stabilities in iso-1-cytochrome *c*. *Protein Sci. 18*, 1155−1164.
(49) Redzic, J. S., and Bowler, B. E. (2005) Role of hydrogen bond networks and dynamics in positive and negative cooperative stabilization of a protein. *Biochemistry 44*, 2900−2908.
(50) Wandschneider, E., Hammack, B. N., and Bowler, B. E. (2003) Evaluation of cooperative interactions between substructures of iso-1-cytochrome *c* using double mutant cycles. *Biochemistry 42*, 10659−10666.
(51) Cherney, M. M., Junior, C., and Bowler, B. E. (2013) Mutation of trimethyllysine-72 to alanine enhances His79-heme mediated dynamics of iso-1-cytochrome *c*. *Biochemistry 52*, 837−846.
(52) Goldes, M. E., Jeakins-Cooley, M. E., McClelland, L. J., Mou, T.-C., and Bowler, B. E. (2016) Disruption of a hydrogen bond network in human versus spider monkey cytochrome *c* affects heme crevice stability. *J. Inorg. Biochem. 158*, 62−69.
(53) Ensign, A. A., Jo, I., Yildirim, I., Krauss, T. D., and Bren, K. L. (2008) Zinc porphyrin: a fluorescent acceptor in studies of Zn-cytochrome *c* unfolding by fluorescence resonance energy transfer. *Proc. Natl. Acad. Sci. U. S. A. 105*, 10779−10784.
(54) Vanderkooi, J. M., Adar, F., and Erecińska, M. (1976) Metallocytochromes *c*: characterization of electronic absorption and

https://dx.doi.org/10.1021/acs.biochem.0c00326
Biochemistry XXXX, XXX, XXX−XXX

emission spectra of Sn^{4+} and Zn^{2+} cytochromes *c*. *Eur. J. Biochem. 64*, 381−387.
(55) Ritchie, T. K., Grinkova, Y. V., Bayburt, T. H., Denisov, I. G., Zolnerciks, J. K., Atkins, W. M., and Sligar, S. G. (2009) Reconstitution of membrane proteins in phospholipid bilayer nanodiscs. *Methods Enzymol. 464*, 211−231.
(56) Nath, A., Atkins, W. M., and Sligar, S. G. (2007) Applications of phospholipid bilayer nanodiscs in the study of membranes and membrane proteins. *Biochemistry 46*, 2059−2069.
(57) Bayburt, T. H., Grinkova, Y. V., and Sligar, S. G. (2002) Self-assembly of discoidal phospholipid bilayer nanoparticles with membrane scaffold proteins. *Nano Lett. 2*, 853−856.
(58) Denisov, I. G., Grinkova, Y. V., Lazarides, A. A., and Sligar, S. G. (2004) Directed self-assembly of monodisperse phospholipid bilayer nanodiscs with controlled size. *J. Am. Chem. Soc. 126*, 3477−3487.
(59) Belikova, N. A., Vladimirov, Y. A., Osipov, A. N., Kapralov, A. A., Tyurin, V. A., Potapovich, M. V., Basova, L. V., Peterson, J., Kurnikov, I. V., and Kagan, V. E. (2006) Peroxidase activity and structural transitions of cytochrome *c* bound to cardiolipin-containing membranes. *Biochemistry 45*, 4998−5009.
(60) Her, C., Filoti, D. I., McLean, M. A., Sligar, S. G., Ross, J. B. A., Steele, H., and Laue, T. M. (2016) The charge properties of phospholipid nanodiscs. *Biophys. J. 111*, 989−998.
(61) Baddam, S., and Bowler, B. E. (2005) Thermodynamics and kinetics of formation of the alkaline state of a Lys 79->Ala/Lys 73->His variant of iso-1-cytochrome c. *Biochemistry 44*, 14956−14968.
(62) Noble, R. W., and Gibson, Q. H. (1970) The reaction of ferrous horseradish peroxidase with hydrogen peroxide. *J. Biol. Chem. 245*, 2409−2413.
(63) Nelson, D. P., and Kiesow, L. A. (1972) Enthalpy of decomposition of hydrogen peroxide by catalase at 25 °C (with molar extinction coefficients of H_2O_2 solutions in the UV). *Anal. Biochem. 49*, 474−478.
(64) Goldschmid, O. (1953) The effect of alkali and strong acid on the ultraviolet absorption spectrum of lignin and related compounds. *J. Am. Chem. Soc. 75*, 3780−3783.
(65) Diederix, R. E. M., Ubbink, M., and Canters, G. W. (2001) The peroxidase activity of cytochrome *c*-550 from *Paracoccus versutus*. *Eur. J. Biochem. 268*, 4207−4216.
(66) Buschmann, V., Krämer, B., Koberling, F., Macdonald, R., and Rüttinge, S. (2009) Quantitative FCS: determination of the confocal volume by FCS and bead scanning with the MicroTime 200. In *Application Note*, pp 1−8, PicoQuant GmbH, Berlin.
(67) Szabelski, M., Luchowski, R., Gryczynski, Z., Kapusta, P., Ortmann, U., and Gryczynski, I. (2009) Evaluation of instrument response functions for lifetime imaging detectors using quenched Rose Bengal solutions. *Chem. Phys. Lett. 471*, 153−159.
(68) Dale, R., Chen, L., and Brand, L. (1977) Rotational relaxation of the 'microviscovity' probe diphenylhexatriene in paraffin oil and egg lecithin vesicles. *J. Biol. Chem. 252*, 7500−7510.
(69) Barkley, M. D., Kowalczyk, A. A., and Brand, L. (1981) Fluorescence decay studies of anisotropic rotations of small molecules. *J. Chem. Phys. 75*, 3581−3593.
(70) Meseth, U., Wohland, T., Rigler, R., and Vogel, H. (1999) Resolution of fluorescence correlation measurements. *Biophys. J. 76*, 1619−1631.
(71) Saffarian, S., and Elson, E. L. (2003) Statistical analysis of fluorescence correlation spectroscopy: the standard deviation and bias. *Biophys. J. 84*, 2030−2042.
(72) Lakowicz, J. R. (2006) *Principles of Fluorescence Spectroscopy*, 3rd ed., Springer, New York.
(73) Bernad, S., Oellerich, S., Soulimane, T., Noinville, S., Baron, M. H., Paternostre, M., and Lecomte, S. (2004) Interaction of horse heart and *Thermus thermophilus* type *c* cytochromes with phospholipid vesicles and hydrophobic surfaces. *Biophys. J. 86*, 3863−3872.
(74) Hong, Y., Muenzner, J., Grimm, S. K., and Pletneva, E. V. (2012) Origin of the conformational heterogeneity of cardiolipin-bound cytochrome *c*. *J. Am. Chem. Soc. 134*, 18713−18723.
(75) Elmer-Dixon, M. M., and Bowler, B. E. (2018) Electrostatic constituents of cardiolipin interaction with site A of cytochrome *c*. *Biochemistry 57*, 5683−5695.
(76) Heimburg, T., and Marsh, D. (1995) Protein surface-distribution and protein-protein interactions in the binding of peripheral proteins to charged lipid membranes. *Biophys. J. 68*, 536−546.
(77) Hobbs, J. K., Jiao, W., Easter, A. D., Parker, E. J., Schipper, L. A., and Arcus, V. L. (2013) Change in heat capacity for enzyme catalysis determines temperature dependence of enzyme catalyzed rates. *ACS Chem. Biol. 8*, 2388−2393.
(78) Lee, J. C., Chang, I. J., Gray, H. B., and Winkler, J. R. (2002) The cytochrome *c* folding landscape revealed by electron-transfer kinetics. *J. Mol. Biol. 320*, 159−164.
(79) Rajagopal, B. S., Silkstone, G. G., Nicholls, P., Wilson, M. T., and Worrall, J. A. R. (2012) An investigation into a cardiolipin acyl chain insertion site in cytochrome *c*. *Biochim. Biophys. Acta, Bioenerg. 1817*, 780−791.
(80) Josephs, T. M., Liptak, M. D., Hughes, G., Lo, A., Smith, R. M., Wilbanks, S. M., Bren, K. L., and Ledgerwood, E. C. (2013) Conformational change and human cytochrome *c* function: mutation of residue 41 modulates caspase activation and destabilizes Met-80 coordination. *JBIC, J. Biol. Inorg. Chem. 18*, 289−297.
(81) Rajagopal, B. S., Edzuma, A. N., Hough, M. A., Blundell, K. L. I. M., Kagan, V. E., Kapralov, A. A., Fraser, L. A., Butt, J. N., Silkstone, G. G., Wilson, M. T., Svistunenko, D. A., and Worrall, J. A. R. (2013) The hydrogen-peroxide-induced radical behaviour in human cytochrome *c*−phospholipid complexes: implications for the enhanced pro-apoptotic activity of the G41S mutant. *Biochem. J. 456*, 441−452.
(82) Pollock, W. B., Rosell, F. I., Twitchett, M. B., Dumont, M. E., and Mauk, A. G. (1998) Bacterial expression of a mitochondrial cytochrome *c*. Trimethylation of Lys72 in yeast iso-1-cytochrome *c* and the alkaline conformational transition. *Biochemistry 37*, 6124−6131.
(83) Kristinsson, R., and Bowler, B. E. (2005) Communication of stabilizing energy between substructures of a protein. *Biochemistry 44*, 2349−2359.
(84) Maity, H., Rumbley, J. N., and Englander, S. W. (2006) Functional role of a protein foldon - an Ω-loop foldon controls the alkaline transition in ferricytochrome *c*. *Proteins: Struct., Funct., Genet. 63*, 349−355.
(85) Cherney, M. M., and Bowler, B. E. (2011) Protein dynamics and function: making new strides with an old warhorse, the alkaline conformational transition of cytochrome *c*. *Coord. Chem. Rev. 255*, 664−677.
(86) Milorey, B., Schweitzer-Stenner, R., Kurbaj, R., and Malyshka, D. (2019) pH-induced switch between different modes of cytochrome *c* binding to cardiolipin-containing liposomes. *ACS Omega 4*, 1386−1400.
(87) Pandiscia, L. A., and Schweitzer-Stenner, R. (2014) Salt as a catalyst in the mitochondria: returning cytochrome *c* to its native state after it misfolds on the surface of cardiolipin containing membranes. *Chem. Commun. 50*, 3674−3676.
(88) Pandiscia, L. A., and Schweitzer-Stenner, R. (2015) Coexistence of native-like and non-native cytochrome *c* on anionic liposomes with different cardiolipin content. *J. Phys. Chem. B 119*, 12846−12859.
(89) Elmer-Dixon, M. M., and Bowler, B. E. (2017) Site A-mediated partial unfolding of cytochrome *c* on cardiolipin vesicles is species-dependent and does not require Lys72. *Biochemistry 56*, 4830−4839.
(90) Kawai, C., Prado, F. M., Nunes, G. L. C., Di Mascio, P., Carmona-Ribeiro, A. M., and Nantes, I. L. (2005) pH-dependent interaction of cytochrome *c* with mitochondrial mimetic membranes: the role of an array of positively charges amino acids. *J. Biol. Chem. 280*, 34709−34717.
(91) Mohammadyani, D., Yanamala, N., Samhan-Arias, A. K., Kapralov, A. A., Stepanov, G., Nuar, N., Planas-Iglesias, J., Sanghera, N., Kagan, V. E., and Klein-Seetharaman, J. (2018) Structural

https://dx.doi.org/10.1021/acs.biochem.0c00326
Biochemistry XXXX, XXX, XXX−XXX

characterization of cardiolipin-driven activation of cytochrome *c* into a peroxidase and membrane perturbation. *Biochim. Biophys. Acta, Biomembr. 1860*, 1057−1068.
(92) Pandiscia, L. A., and Schweitzer-Stenner, R. (2015) Coexistence of native-like and non-native partially unfolded ferricytochrome *c* on the surface of cardiolipin-containing liposomes. *J. Phys. Chem. B 119*, 1334−1349.
(93) Sinibaldi, F., Fiorucci, L., Patriarca, A., Lauceri, R., Ferri, T., Coletta, M., and Santucci, R. (2008) Insights into the cytochrome *c*-cardiolipin interaction. Role played by ionic strength. *Biochemistry 47*, 6928−6935.
(94) Mahajan, N., Hoover, B., Rajendram, M., Shi, H. Y., Kawasaki, K., Weibel, D. B., and Zhang, M. (2019) Maspin binds to cardiolipin in mitochondria and triggers apoptosis. *FASEB J. 33*, 6354−6364.
(95) Kobayashi, H., Nagao, S., and Hirota, S. (2016) Characterization of the cytochrome *c* membrane-binding site using cardiolipin-containing bicelles with NMR. *Angew. Chem., Int. Ed. 55*, 14019−14022.
(96) Bren, K. L. (2016) Going with the electron flow: heme electronic structure and electron transfer in cytochrome *c*. *Isr. J. Chem. 56*, 693−704.
(97) Michel, L. V., Ye, T., Bowman, S. E. J., Levin, B. D., Hahn, M. A., Russell, B. S., Elliott, S. J., and Bren, K. L. (2007) Heme attachment motif mobility tunes cytochrome *c* redox potential. *Biochemistry 46*, 11753−11760.
(98) Kleingardner, J. G., Levin, B. D., Zoppellaro, G., Andersson, K. K., Elliott, S. J., and Bren, K. L. (2018) Influence of heme *c* attachment on heme conformation and potential. *JBIC, J. Biol. Inorg. Chem. 23*, 1073−1083.
(99) Blauer, G., Sreerama, N., and Woody, R. W. (1993) Optical activity of hemoproteins in the Soret region. Circular dichroism of the heme undecapeptide of cytochrome *c* in aqueous solution. *Biochemistry 32*, 6674−6679.
(100) Schweitzer-Stenner, R. (2008) Internal electric field in cytochrome *c* explored by visible electronic circular dichroism spectroscopy. *J. Phys. Chem. B 112*, 10358−10366.
(101) Woody, R. W., and Hsu, M.-C. (1971) The origin of heme cotton effects in myoglobin and hemoglobin. *J. Am. Chem. Soc. 93*, 3515−3525.
(102) Pielak, G. J., Oikawa, K., Mauk, A. G., Smith, M., and Kay, C. M. (1986) Elimination of the native Soret Cotton effect of cytochrome *c* by replacement of the invariant phenylalanine using site-directed mutagenesis. *J. Am. Chem. Soc. 108*, 2724−2727.
(103) Sinibaldi, F., Droghetti, E., Polticelli, F., Piro, M. C., Di Pierro, D., Ferri, T., Smulevich, G., and Santucci, R. (2011) The effects of ATP and sodium chloride on the cytochrome *c*−cardiolipin interaction: The contrasting behavior of the horse heart and yeast proteins. *J. Inorg. Biochem. 105*, 1365−1372.
(104) Sinibaldi, F., Howes, B. D., Droghetti, E., Polticelli, F., Piro, M. C., Di Pierro, D., Fiorucci, L., Coletta, M., Smulevich, G., and Santucci, R. (2013) Role of lysines in cytochrome *c*−cardiolipin interaction. *Biochemistry 52*, 4578−4588.
(105) Sinibaldi, F., Howes, B. D., Piro, M. C., Polticelli, F., Bombelli, C., Ferri, T., Coletta, M., Smulevich, G., and Santucci, R. (2010) Extended cardiolipin anchorage to cytochrome *c*: a model for protein-mitochondrial membrane binding. *JBIC, J. Biol. Inorg. Chem. 15*, 689−700.
(106) Elmer-Dixon, M. M. (2018) Elucidation of the physical and chemical properties of cytochrome c-cardiolipin interactions. Ph.D. Thesis, Biochemistry & Biophysics Graduate Program, Missoula, MT.
(107) Verbaro, D., Hagarman, A., Soffer, J., and Schweitzer-Stenner, R. (2009) The pH dependence of the 695 nm charge transfer band reveals the population of an intermediate state of the alkaline transition of ferricytochrome *c* at low ion concentrations. *Biochemistry 48*, 2990−2996.
(108) Junedi, S., Yasuhara, K., Nagao, S., Kikuchi, J.-I., and Hirota, S. (2014) Morphological change of cell membrane by interaction with domain-swapped cytochrome *c* oligomers. *ChemBioChem 15*, 517−521.
(109) Green, D. R. (2005) Apoptotic pathways: ten minutes to dead. *Cell 121*, 671−674.
(110) Nold, S. M., Lei, H., Mou, T.-C., and Bowler, B. E. (2017) Effect of a K72A mutation on the structure, stability, dynamics and peroxidase activity of human cytochrome *c*. *Biochemistry 56*, 3358−3368.
(111) Muenzner, J., Toffey, J. R., Hong, Y., and Pletneva, E. V. (2013) Becoming a peroxidase: cardiolipin-induced unfolding of cytochrome *c*. *J. Phys. Chem. B 117*, 12878−12886.
(112) Radi, R., Thomson, L., Rubbo, H., and Prodanov, E. (1991) Cytochrome *c*-catalyzed oxidation of organic molecules by hydrogen peroxide. *Arch. Biochem. Biophys. 288*, 112−117.
(113) Xu, Y., Mayne, L., and Englander, S. W. (1998) Evidence for an unfolding and refolding pathway in cytochrome *c*. *Nat. Struct. Biol. 5*, 774−778.
(114) Adams, P. A., Baldwin, D. A., and Marques, H. M. (1996) The hemepeptides from cytochrome *c*: Preparation, physical and chemical properties, and their use as model compounds for the hemoproteins. In *Cytochrome c: A Multidisciplinary Approach* (Mauk, A. G., and Scott, R. A., Eds.) pp 635−692, University Science Books, Sausalito, CA.
(115) Diederix, R. E. M., Ubbink, M., and Canters, G. W. (2002) Peroxidase activity as a tool for studying the folding of *c*-type cytochromes. *Biochemistry 41*, 13067−13077.
(116) Laun, P., Buettner, S., Rinnerthaler, M., Burhans, W. C., and Breitenbach, M. (2012) Yeast Aging and Apoptosis. In *Subcellular Biochemistry: Aging Research in Yeast* (Breitenbach, M., Jazwinski, S. M., and Laun, P., Eds.) pp 207−232, Springer, Dordrecht, The Netherlands.
(117) Porcelli, A. M., Ghelli, A., Zanna, C., Pinton, P., Rizzuto, R., and Rugolo, M. (2005) pH difference across the outer mitochondrial membrane measured with a green fluorescent protein mutant. *Biochem. Biophys. Res. Commun. 326*, 799−804.
(118) Nilsson, C., Kågedal, K., Johansson, U., and Öllinger, K. (2004) Analysis of cytosolic and lysosomal pH in apoptotic cells by flow cytometry. *Methods Cell Sci. 25*, 185−194.
(119) Hackenbrock, C. R., Chazotte, B., and Gupte, S. S. (1986) The random collision model and a critical assessment of diffusion and collision in mitochondrial electron transport. *J. Bioenerg. Biomembr. 18*, 331−368.
(120) Garber Morales, J., Holmes-Hampton, G. P., Miao, R., Guo, Y., Münck, E., and Lindahl, P. A. (2010) Biophysical characterization of iron in mitochondria isolated from respiring and fermenting yeast. *Biochemistry 49*, 5436−5444.

https://dx.doi.org/10.1021/acs.biochem.0c00326
Biochemistry XXXX, XXX, XXX−XXX